Correlated Multiple Sampling impact analysis on 1/fE noise for image sensors

A. Peizerat, G. Renaud

▶ **To cite this version:**

A. Peizerat, G. Renaud. Correlated Multiple Sampling impact analysis on 1/fE noise for image sensors. Journal of Electronic Imaging, 2019, 31 (9), pp.368-1-368-6. 10.2352/ISSN.2470-1173.2019.9.IMSE-368 . cea-04548728

HAL Id: cea-04548728

https://cea.hal.science/cea-04548728

Submitted on 16 Apr 2024

HAL is a multi-disciplinary open access archive for the deposit and dissemination of scientific research documents, whether they are published or not. The documents may come from teaching and research institutions in France or abroad, or from public or private research centers.

L'archive ouverte pluridisciplinaire **HAL**, est destinée au dépôt et à la diffusion de documents scientifiques de niveau recherche, publiés ou non, émanant des établissements d'enseignement et de recherche français ou étrangers, des laboratoires publics ou privés.

Correlated Multiple Sampling impact analysis on 1/f^E noise for image sensors

A. Peizerat, G. Renaud, CEA-LETI, Grenoble, France

Abstract

Correlated Multiple Sampling (CMS), which is an extension of Correlated Double Sampling (CDS), is a very popular noise reduction technique used in the readout chain of image sensors. It has been analyzed in the literature, showing that, with an increasingly number M of samples, the total noise tends to a limit value dominated by the pixel 1/f noise. Nevertheless, this approach fails to explain why, in some cases, the total noise measurement may reach a minimum before, against all odds, finally growing with M. This paper shows that an explanation can be found if the pixel noise Power Spectral Density (PSD) varies in 1/f^E with a frequency exponent E > 1 instead of E=1.

Index Terms— Image sensor, 1/f noise, Correlated Double Sampling, Correlated Multiple Sampling, pixel

INTRODUCTION

The low noise feature is a growing need for an image sensor as it determines its low light performance, which is of critical interest in applications like automotive, surveillance, scientific imaging or space. Several papers report an Input Referred Temporal Noise (IRTN) below the electron value like in [1] where process and design are optimized. Among the noise reduction techniques that have been studied [2], a particular one, the Correlated Multiple Sampling (CMS), raised large interest from the imaging community. Its impact on the noise is well documented [3-9], showing that, except for high speed imagers, the remaining noise is the 1/f noise. The behavior of this remaining noise is predicted by an analysis based on an ideal pixel Power Spectral Density (PSD) following a 1/f^E curve with a frequency exponent E strictly equal to 1. Previously published works [10-12] showed that E can be measured somewhere in between 0.7 and 1.3, those variations being mainly due to the oxide nature and its spatial distribution of traps. Contrary to [3-9], the present paper gives an insight of the CMS impact for a pixel exhibiting a 1/f^E noise with E≠1.

First, the CMS analysis, when taking into account an exponent E≠1, is described. Then, a numerical example is given. Finally, it is shown how this analysis applies to measurement coming from an image sensor test chip.

CMS analysis

A classic low noise image sensor readout chain is given in Fig. 1. A 4T pixel is followed by a Programmable Gain Amplifier (PGA) that feeds a CMS block:

- The PGA, thanks to its gain, makes all the subsequent noise sources negligible. Its cut-off frequency, f_C, is smaller than that of the pixel so that f_C defines the bandwidth just before the CMS block.
- The CMS block performs the difference between the signal average before and after the charge transfer of the pixel. Each average is computed on M samples with a sampling period of T_{CMS}. This CMS operation can be done in the analog or digital domain but this point is not discussed here, assuming ideal sampling and averaging.

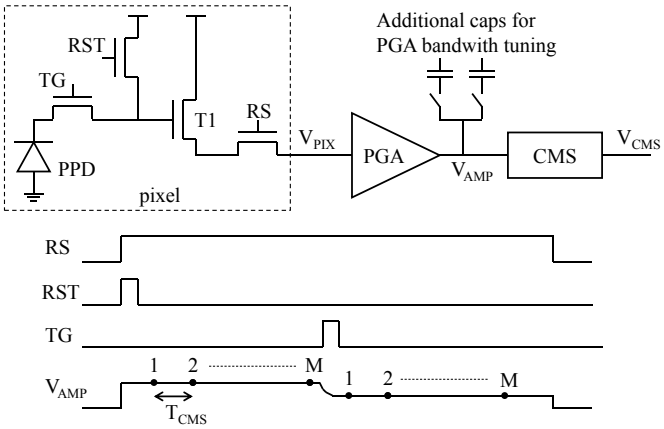

Fig. 1 A classic low noise image sensor readout chain [2] and its associated timing diagram where a 4T pixel is followed by a M-order CMS: M samples are used to average the signal before and after the TG pulse then a subtraction is performed.

Fig. 2 shows the noise path from the pixel follower transistor channel, which is the main noise contributor [2], to the CMS output. In the frequency domain, $H_{N,readout}(f)$ is the transfer function between the T1 channel noise current source I_N and the CMS block input $V_{N,AMP}$. This transfer function is easily broken down into two pieces [2]: a DC gain related to the readout chain DC gain and a unity gain lowpass filter whose cut-off frequency is f_C.

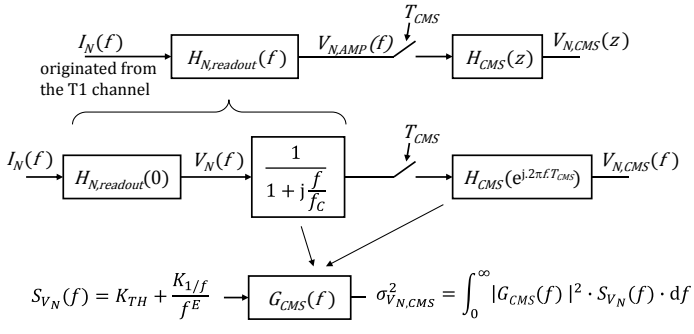

Fig. 2 Noise path from the follower transistor T1 channel (on Fig. 1) to the CMS ouput and definition of the transfer function G_{CMS} : G_{CMS} includes the readout chain unity gain lowpass filter and the CMS highpass filter.

In order to assess $\sigma^2_{V_{N,CMS}}$, the RMS output voltage noise, the total CMS transfer function G_{CMS} is defined as the product of this unity gain lowpass filter and the transfer function of the CMS block H_{CMS} so as to obtain the G_{CMS} modulus squared [13]:

$$|G_{CMS}(f)|^2 = \frac{1}{1+\left(\frac{f}{f_C}\right)^2} \cdot \frac{4}{M^2} \cdot \frac{\sin^4(\pi f M T_{CMS})}{\sin^2(\pi f T_{CMS})} \qquad (1)$$

For the sake of simplicity, $|G_{CMS}(f)|^2$ does not include the periodic repetition of the spectrum as sampling has no impact on the signal power. The noise power can be then given by:

$$\sigma^2_{V_{N,CMS}} = \int_0^\infty |G_{CMS}(f)|^2 \cdot S_{V_N}(f) \cdot \mathrm{d}f \qquad (2)$$

Where S_{V_N} is the input single-sided Power Spectral Density (PSD) of the T1 noise current source amplified by $H_{N,readout}(0)$. S_{V_N} can be divided into a thermal part and a 1/f part as follows:

$$S_{V_N}(f) = K_{TH} + \frac{K_{1/f}}{f^E} \qquad (3)$$

Where K_{TH}, $K_{1/f}$ and E are constants depending on the used CMOS process, the pixel layout as well as the size and biasing of the source follower transistor [2].

Numerical integration allows the calculation of equation (2), leading to equation (4) that gives the resulting noise at the CMS output. It consists in a well-known thermal noise contribution and a new 1/f noise contribution:

$$\sigma^2_{V_{N,CMS}} = \alpha_{TH} \cdot \frac{\pi f_C}{M} \cdot K_{TH} + \alpha_{1/f} \cdot \frac{1}{f_C^{E-1}} \cdot K_{1/f} \qquad (4)$$

with $\alpha_{TH} = \frac{M}{\pi . f_C} \cdot \int_0^\infty |G_{CMS}(f)|^2 \cdot \mathrm{d}f$

and $\alpha_{1/f} = f_C^{E-1} \cdot \int_0^\infty |G_{CMS}(f)|^2 \cdot \frac{1}{f^E} \cdot \mathrm{d}f$

The two parameters, α_{TH} and $\alpha_{1/f}$, are used to simplify the interpretation of (4):

– α_{TH} is of course not impacted by E value and $\alpha_{TH} \approx 1$ if $2\pi f_C T_{CMS} > 6$, which is the common case in order to allow sufficient settling of the signal between two samples [13].

– $\alpha_{1/f}$ cannot be given by a set of curves as a function of $2\pi f_C T_{CMS}$ and parametrized only by M, like in [13]. It has to be also parametrized by E as illustrated by the new different curves on Fig. 3.

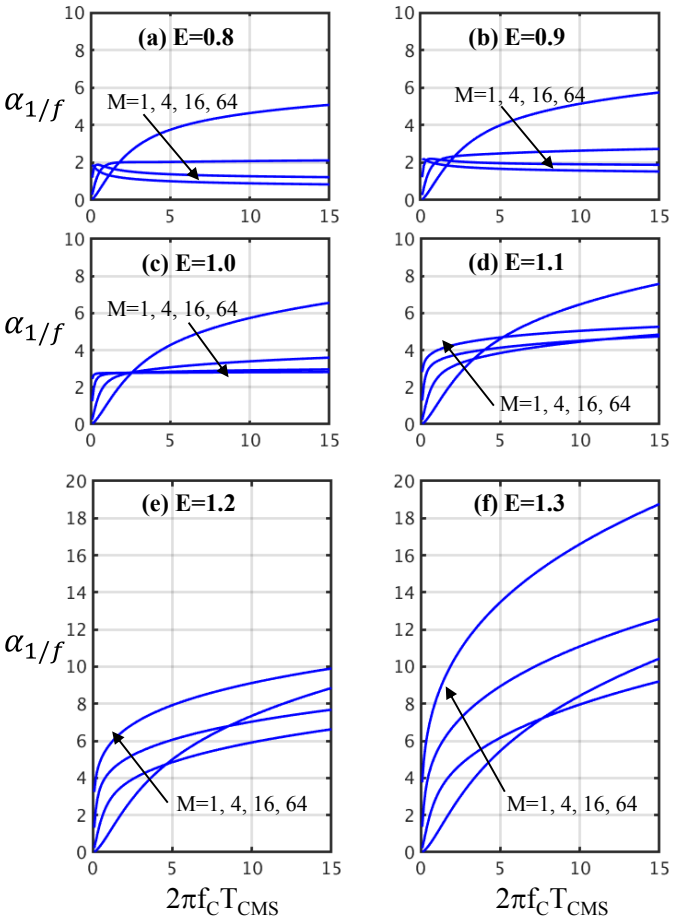

Fig. 3 $\alpha_{1/f}$ as defined in (4) resulting from a numerical integration for different value of the exponent E: (c) shows the well-known curves when E=1 [13]. (a), (b), (d), (e) and (f) show the $\alpha_{1/f}$ curves for E=0.8, 0.9, 1.1, 1.2 and 1.3, respectively.

For E values lower than 1, Fig. 3(a) and Fig. 3(b) show $\alpha_{1/f}$ curves with a behavior similar to the case E=1 of Fig. 3(c): the greater the M value, the lower $\alpha_{1/f}$, so the lower the 1/f noise contribution. The difference between those cases lies into the absolute $\alpha_{1/f}$ value that decreases with E: E=1 best curve gives $\alpha_{1/F} \sim 3$ whereas E=0.8 best curve gives $\alpha_{1/F} \sim 1$.

For E values greater than 1, Fig. 3 illustrates that a high value for M no longer guarantees the lowest 1/f noise. For the case E=1.2 of Fig. 3(e) and for a T_{CMS} value given by $2\pi f_C T_{CMS} \approx 10$, the order M=4 gives less noise than M=16 and M=64. The case E=1.3, Fig. 3(f), shows that the order M=1, a simple CDS, is not only better than M=16 and M=64 but also nearly as efficient as M=4.

Another interesting result given by (4) lies in the fact that, in spite of a constant value for $\alpha_{1/f}$ (i.e. constant values for $2\pi f_C T_{CMS}$ and M), the 1/f noise contribution increases as the parameter f_C decreases if E >1. The 1/f noise CMS optimization may then not be a high value for M and a low value for f_C but will result from a trade-off between those two parameters.

Numerical example

Some parameters have been set so as to show a realistic example of the previously-described analysis:

- $K_{TH}= 5.10^{-14}$ (V^2/Hz),
- $K_{1/f}$ (V^2/Hz) is chosen accordingly to the E value so that the corner frequency stays the same, about 100kHz, as illustrated on Figure 4,
- $2\pi f_C T_{CMS}= 15$,

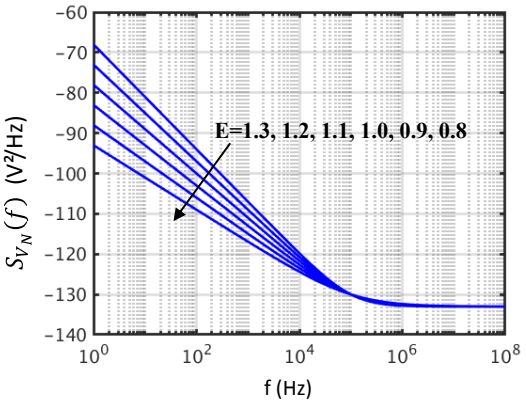

Fig. 4 Bode diagram of the PSD S_{V_N} of equation (3) with $K_{TH}= 5.10^{-14}$ and a 100kHz corner frequency

With that set of parameter values, the impact of CMS on the different noises is illustrated on Figure 5 for f_C=450kHz. The thermal noise contribution, $\sigma_{V_{N,TH,CMS}}$, is not impacted by E and is inversely proportional to the square root of M. On the other hand, the 1/f noise contribution, $\sigma_{V_{N,1/f,CMS}}$, can increase with M if E > 1. The total noise, $\sigma_{V_{N,CMS}}$, which is the quadratic summation of those two latter noises, can be improved or deteriorated with M according to E values.

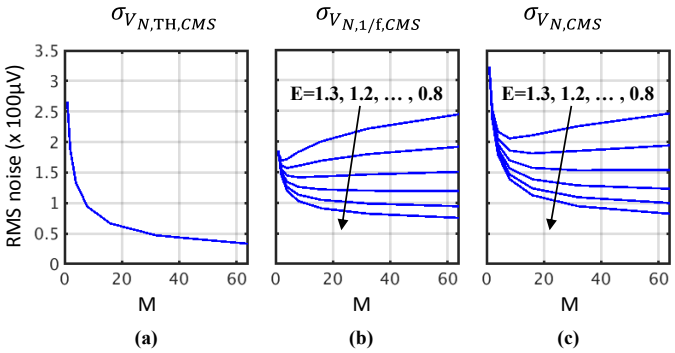

Fig. 5 Resulting RMS output noises as a function of M, after numerical integration of equation (4) for the input PSD S_{V_N} of Figure 4, with f_C= 450kHz and T_{CMS}= 5.3µs. (a) gives the thermal noise contribution, (b) gives the 1/f noise contribution and (c) gives the total output noise.

In that particular numerical example, CMS is mainly useful to reduce the thermal noise contribution until the 1/f noise contribution prevails. At that very point, if E > 1, increasing M value can result in a total noise increase.

With the same set of parameters ($2\pi f_C T_{CMS}= 15$, K_{TH}, $K_{1/f}$), we can assess the influence of f_C, the PGA cut-off frequency. Figure 6 gives the same noise contributions as Figure 5 but for M=8 and as a function of f_C.

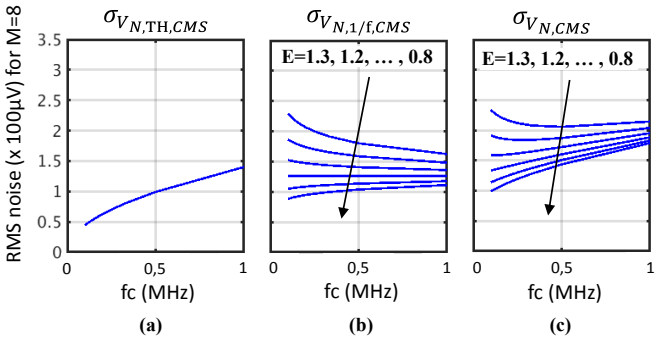

Fig. 6 Resulting RMS output noises after numerical integration of equation (4) for the input PSD S_{V_N} of Figure 4, for M=8 and a varying f_C. (a) gives the thermal noise contribution, (b) gives the 1/f noise contribution and (c) gives the total output noise.

If E < 1, a small f_C (at $2\pi f_C T_{CMS}$= constant) reduces both the thermal and the 1/f noises. If E ≥ 1, the thermal noise benefits from a small f_C whereas the 1/f noise benefits from a large f_C, meaning a minimum total output noise can be found for a given M. For example, as illustrated on Figure 6 (c) for E=1.3, a minimum total output noise of ~200 µV is reached for $f_C \approx$ 500 kHz,

Test-chip results

The test-chip has been fabricated in a 90nm CIS CMOS process, its photography is given on Fig. 7. Different pixels have been implemented in the matrix of a generic frame called "Creapyx" developed by the company Pyxalis [14]. This versatile frame is designed to provide flexible readout schemes for a fast prototyping of a wide range of pixel types. It outputs analog values that are converted to digital domain thanks to a 16-bit ADC implemented on the associated board. Among six different 4T pixel versions, two are of interest for the purpose of this paper, each pixel version implemented in a 40x400 pixel array. These two pixels have a 6.5µm pitch, use thick oxide transistors and aim at low-noise performance, the differences lying mainly in the follower transistor features.

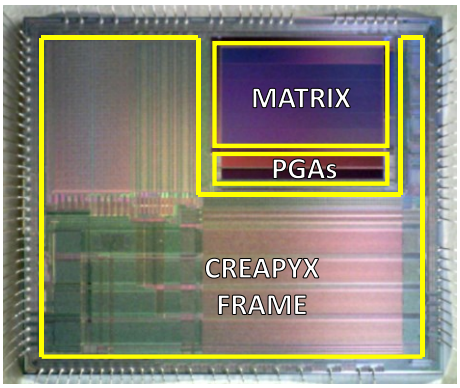

Fig. 7 Die photography

As this circuit was not initially intended for CMS measurement, only CDS is available. The adjustable bandwidth f_C is then exploited to make equation (4) match the noise behavior of the measured pixel.

The pixel Conversion Gain (CG), useful to input-referred the output noise, is assessed thanks to the Photon Transfer Curve (PTC): through different uniform illuminations. The curve of the signal variance as a function of the signal average gives, Fig. 8, the pixel CG [15].

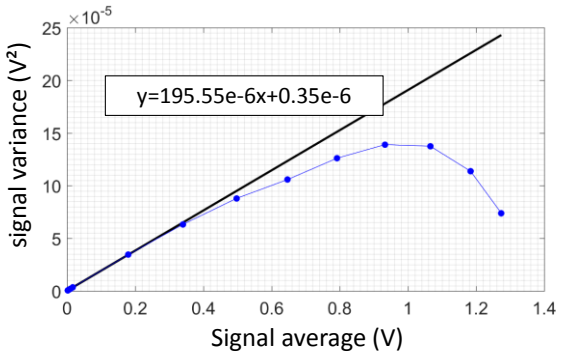

Fig. 8 Example of a Photon Transfer Curve (in blue) measured for a pixel of the test-chip with a PGA gain of 1. The tangent slope at the origin gives the average conversion gain in low-light conditions. For that case: 195µV/e-

Concerning the Input Referred Temporal Noise (IRTN) evaluation, the sensor is put in dark conditions without pulsing the TG signal during the readout in order to rule out noise originated from the dark current or the TG gate. The temporal standard deviation (RMS noise) per pixel is assessed thanks to 100 measurements, then at least 10,000 pixels per pixel version are used to build the input referred noise histogram. The histogram peak gives a good estimate of the total noise for a given pixel version as illustrated Fig. 9.

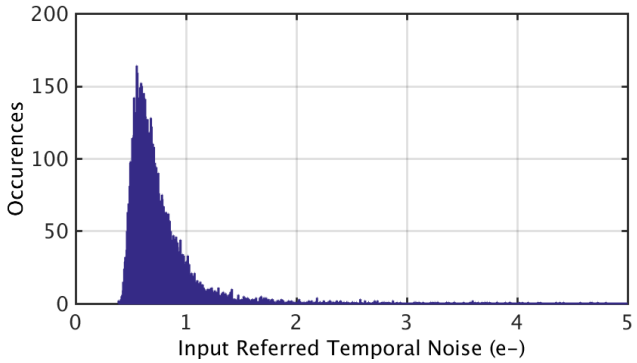

Fig. 9 Example of an IRTN histogram whose peak is used as an estimate of the noise that does not take into account non-studied pixel behaviors (e.g. Random Telegraph Signal noise)

Table 1: Measured IRTN for 3 different f_C at $2\pi f_C T_{CMS}$=constant

Pixel version	CG	T_{CMS}	f_C	Measured IRTN
Pixel 1	195µV/e-	5µs	450kHz	0.55e-
		15µs	150kHz	0.64e-
		45µs	50kHz	0.69e-
Pixel 2	140µV/e-	5µs	450kHz	0.56e-
		15µs	150kHz	0.63e-
		45µs	50kHz	0.68e-

Noise results are shown in Table 1 for the order M=1 (i.e. a simple CDS), with $2\pi f_C T_{CMS}$=constant and for 3 different values for f_C, f_C being tuned thanks to different capacitances at the PGA output (Fig. 1). Despite the fact that pixel versions have a significant different CG, the measured IRTN show the same behavior. The classic noise formula (equivalent to Equation (4) with E=1, [8, 13]) predicts a smaller contribution of the thermal noise (as f_C decreases and α_{TH}, M and K_{TH} remain the same) and a constant contribution of the 1/f noise (as K_{TH} and $\alpha_{1/f}$ remain the same). So it fails to explain the increasing measured noise when f_C decreases. On the contrary, Equation (4) with M=1 and E>1 can explain such a behavior. For that purpose, (4) can be written also as:

$$IRTN = \sqrt{\frac{f_C}{f_0} \cdot N_{TH\_0}^2 + \left(\frac{f_0}{f_C}\right)^{E-1} \cdot N_{1/F\_0}^2} \qquad (5)$$

Where f_0=450kHz is the typical value of f_C, N_{TH_0} is the IRTN due to thermal noise for $f_C=f_0$ and N_{1/F_0} is the IRTN due to 1/f noise for $f_C=f_0$. Table 2 gives E, N_{TH_0} and N_{1/F_0} values that make predicted IRTN from equation (5) match measured IRTN from Table 1. A value of 1.3 for the exponent E seems as a good candidate to explain why measured IRTN increases when f_C decreases.

Table 2: Predicted IRTN according to equation (5) for the empirical values E=1.3, N_{TH_0}=0.21e- and N_{1/F_0}=0.52e-.

E	N_{TH_0}	N_{1/F_0}	f_0/f_C	Predicted IRTN
1.3	*0.21e-*	*0.52e-*	1	0.56e-
			3	0.63e-
			6	0.69e-

Conclusion

This paper analyses the CMS response to a 1/f noise whose PSD would be in $1/f^E$. The derived new equation (4) shows that the case E=1 and cases E<1 present roughly the same behaviors. On the contrary, if E>1, the minimum resulting 1/f noise may not be obtained necessarily with a high value for M (CMS order) or a low value for f_C (CMS input bandwith). The optimization will result from a trade-off between those two parameters. For the process and the transistors used on our test-chip, the presented CMS analysis shows that a value of 1.3 for E seems to be a good candidate in order for the analytical results to match the measured ones.

Acknowledgment

The authors would like to thank Pyxalis (Moirans, France) for validating the technical work in the frame of a partnership on this topic.

References

[1] M.-W. Seo, S. Kawahito, K. Kagawa, and K. Yasutomi, “A 0.27 e− rms read noise 220 μV/e− conversion gain reset-gate-less CMOS image sensor with 0.11 μm CIS process”, IEEE EDL , vol. 36, no. 12, pp. 1344–1347, Dec. 2015.

[2] A. Boukhayma, A. Peizerat and C. Enz: "Temporal Readout Noise Analysis and Reduction Techniques for Low-Light CMOS Image Sensors", in IEEE TED, vol. 63, no. 1, pp. 72-78, Jan. 2016, doi : 10.1109/TED.2015.2434799

[3] S. Suh, S. Itoh, S. Aoyama, and S. Kawahito, “Column-parallel correlated multiple sampling circuits for CMOS image sensors and their noise reduction effects”, Sensors, vol. 10, no. 10, pp. 9139–9154, Oct. 2010. doi:10.3390/s101009139

[4] S. F. Yeh, K. Y. Chou, H. Y. Tu, C. Y. P. Chao and F. L. Hsueh, "A 0.66erms− Temporal-Readout-Noise 3-D-Stacked CMOS Image Sensor With Conditional Correlated Multiple Sampling Technique", in IEEE JSSC, vol. 53, no. 2, pp. 527-537, Feb. 2018. doi: 10.1109/JSSC.2017.2765927

[5] Y. Chen, Y. Xu, Y. Chae, A. Mierop, X. Wang, and A. Theuwissen, “A 0.7 e−rms-temporal-readout-noise CMOS image sensor for lowlight-level imaging”, in IEEE ISSCC Dig. Tech. Papers, Feb. 2012, pp. 384–385. DOI: 10.1109/ISSCC.2012.6177059

[6] Swaraj Mahato, Guy Meynants, Gert Raskin, J. De Ridder, H. Van Winckel, "Noise optimization of the source follower of a CMOS pixel using BSIM3 noise model”, SPIE Proceedings, 2016, arXiv:1609.04315

[7] Kawahito, S.; Seo, M.-W, “Noise Reduction Effect of Multiple-Sampling-Based Signal-Readout Circuits for Ultra-Low Noise CMOS Image Sensors”, 16, 1867, Sensors 2016, doi:10.3390/s16111867

[8] N. Kawai, S. Kawahito, "Effectiveness of a correlated multiple sampling differential averager for reducing 1/f noise", IEICE Electronics Express Letter, 2005, doi: https://doi.org/10.1587/elex.2.379

[9] A. Boukhayma, A. Peizerat, and C. Enz, “A sub-0.5 electron read noise VGA image sensor in a standard CMOS process,” IEEE J. SolidState Circuit, vol. 51, no. 9, pp. 2180–2190, Sep. 2016, doi: 10.1109/ JSSC.2016.2579643.

[10] Y. Nemirovsky, D. Corcos, I. Brouk, A. Nemirovsky and S. Chaudhry, "1/f noise in advanced CMOS transistors," in IEEE Instrumentation & Measurement Magazine, vol. 14, no. 1, pp. 14-22, Feb. 2011. doi: 10.1109/MIM.2011.5704805

[11] K.W. Chew, K.S. Yeo, S.-F. Chu, “Effect of technology scaling on the 1/f noise of deep submicron PMOS transistors”, Solid-State Electronics, Volume 48, Issue 7, 2004, Pages 1101-1109, ISSN 0038-1101, https://doi.org/10.1016/j.sse.2004.02.009

[12] E. Simoen, C. Claeys, “On the flicker noise in submicron silicon MOSFETs”, Solid-State Electronics, Volume 43, Issue 5, 1999, Pages 865-882, ISSN 0038-1101, https://doi.org/10.1016/S0038-1101(98)00322-0

[13] A. Boukhayma, A. Peizerat, A. Dupret and C. Enz, "Design optimization for low light CMOS image sensors readout chain", IEEE NEWCAS 2014, pp. 241-244, DOI: 10.1109/NEWCAS.2014.6934028

[14] http://www.pyxalis.com/pyxalis-wp/wp-download/publications/2015_PYXALIS_CNES_CREAPYX.pdf

[15] J. R. Janesick, “Photon Transfer Theory” in Photon Transfer, SPIE PRESS BOOK, Aug. 2007, ISBN: 9780819467225